LISA Sensitivity

Neil J. Cornish

The goal of this document is to explain the construction and use of LISA sensitivity curves, the computation of signal-to-noise ratios, and how to plot signal strengths against the sensitivity curve. Figure 1 shows an example of a sensitivity/source plot taken from the LISA L3 mission proposal [1]. The idea is that the height a signal is above the sensitivity curve indicates how loud it will be.

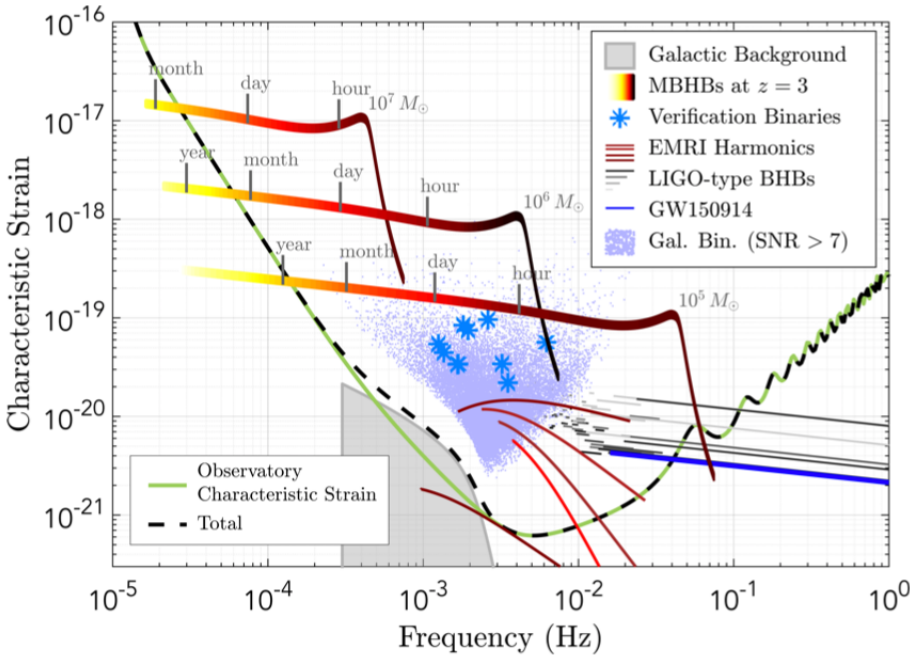

Figure 1: A plot taken from the LISA L3 mission proposal showing the expected sensitivity (green line) and a variety of possible sources (various colors) in units of dimensionless characteristic strain.

The literature on this topic can be very confusing, with a profusion of conventions and notation. Unfortunately some of the choices that have now become standard are misleading, but it is probably too late to change now. Sensitivity curves are useful for making a quick assessment of what signals may be detectable. While not used for actual data analysis, the sensitivity curve, and signal representations that are shown with them, are designed to represent the quantities that are used in the data analysis. See Ref. [2] for a review of gravitational wave sensitivity curves.

1 Sensitivity Curves

For those in a hurry, or for those that already know everything there is to know about sensitivity curves, the following equation provides a very good analytic fit to the current (as of February 2018)

official LISA sensitivity curve:

$$S_n(f) = \frac{10}{3L^2}\left(P_{\rm OMS}(f) + \frac{4P_{\rm acc}(f)}{(2\pi f)^4}\right)\left(1 + \frac{6}{10}\left(\frac{f}{f_*}\right)^2\right) + S_c(f)\,, \tag{1}$$

where $L = 2.5$ Gm, $f_* = 19.09$ mHz, and expressions for $P_{\rm OMS}(f)$, $P_{\rm acc}(f)$ and $S_c(f)$ are given in equations (10), (11) and (14) below. For those that would like to know more, please read on.

The simplest type of sensitivity curve, and the one used by the ground-based detector community, is the power spectral density of the detector noise $P_n(f)$, or the amplitude spectral density $\sqrt{P_n(f)}$. The mean-squared noise in the frequency band $[f_1, f_2]$ is just the integral of $P_n(f)$ over that band. But for a detector like LISA, where signals may have wavelengths that are longer than the arms of the detector, it is conventional to include the ensuing arm-length penalty in the sensitivity curve [3]. The strain spectral sensitivity is then defined in terms of the square root of the effective noise power spectral density

$$S_n(f) = \frac{P_n(f)}{\mathcal{R}(f)}, \tag{2}$$

where $\mathcal{R}(f)$ is the sky and polarization averaged signal response function of the instrument. The signal response function $\mathcal{R}(f)$ relates the power spectral density of the incident gravitational wave signals to the power spectral density of the signal recorded in the detector. As such, it might have been more logical to include this factor in the expression of the signals, but early on it was decided to apply the inverse of this factor to the noise power to define a sensitivity curve - C'est la vie.

The response function can be computed by working in the frequency domain, where the gravitational wave amplitude in the detector, $\tilde{h}(f)$, is related to the plus and cross gravitational wave amplitudes via

$$\tilde{h}(f) = F^+(f)\tilde{h}_+(f) + F^\times(f)\tilde{h}_\times(f)\,, \tag{3}$$

where $F^+(\theta,\phi,\psi,f)$ and $F^\times(\theta,\phi,\psi,f)$ are the (complex) frequency dependent detector response functions, which depend on the sky location (θ,ϕ) and polarization angle ψ of the source. The sky/polarization averaged spectral power of the signal in the detector, $\langle\tilde{h}(f)\tilde{h}^*(f)\rangle$ is related to the raw spectral signal power $|\tilde{h}_+(f)|^2 + |\tilde{h}_\times(f)|^2$ by the response function:

$$\begin{aligned}\langle\tilde{h}(f)\tilde{h}^*(f)\rangle &= \langle F^+(f)F^{+*}(f)\rangle|\tilde{h}_+(f)|^2 + \langle F^\times(f)F^{\times*}(f)\rangle|\tilde{h}_\times(f)|^2 \\ &= \mathcal{R}(f)\left(|\tilde{h}_+(f)|^2 + |\tilde{h}_\times(f)|^2\right)\end{aligned} \tag{4}$$

where $\mathcal{R}(f) = \langle F^+(f)F^{+*}(f)\rangle = \langle F^\times(f)F^{\times*}(f)\rangle$, and the angle brackets indicate the sky/polarization average

$$\langle X\rangle \equiv \frac{1}{4\pi^2}\int_0^\pi d\psi \int_0^{2\pi} d\phi \int_0^\pi X\,\sin\theta\, d\theta. \tag{5}$$

For a right-angle interferometer operating in the long wavelength limit, such as LIGO/Virgo, the antenna patterns are real and independent of frequency, and are given by

$$\begin{aligned}F^+ &= \frac{1}{2}(1+\cos^2\theta)\cos(2\phi)\cos(2\psi) - \cos\theta\sin 2\phi\sin 2\psi \\ F^\times &= \frac{1}{2}(1+\cos^2\theta)\cos(2\phi)\sin(2\psi) + \cos\theta\sin 2\phi\cos 2\psi\end{aligned} \tag{6}$$

For LIGO we have

$$\mathcal{R} = \langle {F^+}^2 \rangle = \langle {F^\times}^2 \rangle = \frac{1}{32} \int_{-1}^{1} (1 + 6x^2 + x^4) dx = \frac{1}{5} \,. \tag{7}$$

In the LIGO literature this factor is applied to the signals, leaving the sensitivity curve to be just the power spectral density of the noise. The full expressions for $F^+(f)$ and $F^\times(f)$ for the Michelson-style interferometry signals for LISA are much more complicated than those for LIGO (they are given in equations (5), (6), (16) and (17) of Ref. [4].) For a 3-arm LISA, there are two independent channels for $f < f_*$ and three for $f > f_*$, where $f_* = c/(2\pi L)$ is the transfer frequency [5]. For the current LISA design, $L = 2.5$ Gm, and $f_* = 19.09$ mHz. The standard convention is to define $\mathcal{R}(f)$ as being summed over the plus and cross channels. For sources that have frequency components $f > f_*$, it is more accurate to consider the 3-channel expressions given in Ref. [5]. The full expression for $\mathcal{R}(f)$ is not known in closed form for LISA, but to leading order is given by

$$\mathcal{R}(f) = \frac{3}{10} - \frac{507}{5040} \left(\frac{f}{f_*} \right) + \ldots \tag{8}$$

The first term, $3/10$, is a factor of $2 \times \sin^2(60^\circ) = 3/2$ larger than the corresponding LIGO result due to the LISA having two low-frequency channels, and arms that make an angle of 60°, as opposed to the 90° angle for LIGO. The full expression for $\mathcal{R}(f)$ has to be computed numerically [3], and has the form shown in Figure 2. The transfer function can be well-fit by the curve

$$\mathcal{R}(f) = \frac{3}{10} \frac{1}{(1 + 0.6(f/f_*)^2)} \tag{9}$$

Note that many publications quote the number $3/20$ for the low frequency limit of $R(f)$. The factor of two larger value quoted here comes from summing over the two independent low-frequency data channels.

The current "official" model for the power spectral density of the LISA noise $P_n(f)$ is based on the Payload Description Document, and is referenced in the "LISA Strain Curves" document LISA-LCST-SGS-TN-001. The single-link optical metrology noise is quoted as

$$P_{\rm OMS} = (1.5 \times 10^{-11}\,{\rm m})^2 \left(1 + \left(\frac{2\,{\rm mHz}}{f} \right)^4 \right) \,{\rm Hz}^{-1} \,, \tag{10}$$

and the single test mass acceleration noise is quoted as

$$P_{\rm acc} = (3 \times 10^{-15}\,{\rm m\,s^{-2}})^2 \left(1 + \left(\frac{0.4\,{\rm mHz}}{f} \right)^2 \right) \left(1 + \left(\frac{f}{8\,{\rm mHz}} \right)^4 \right) \,{\rm Hz}^{-1} \,. \tag{11}$$

The total noise in a Michelson-style LISA data channel is then [4]

$$P_n(f) = \frac{P_{\rm OMS}}{L^2} + 2(1 + \cos^2(f/f_*)) \frac{P_{\rm acc}}{(2\pi f)^4 L^2} \,. \tag{12}$$

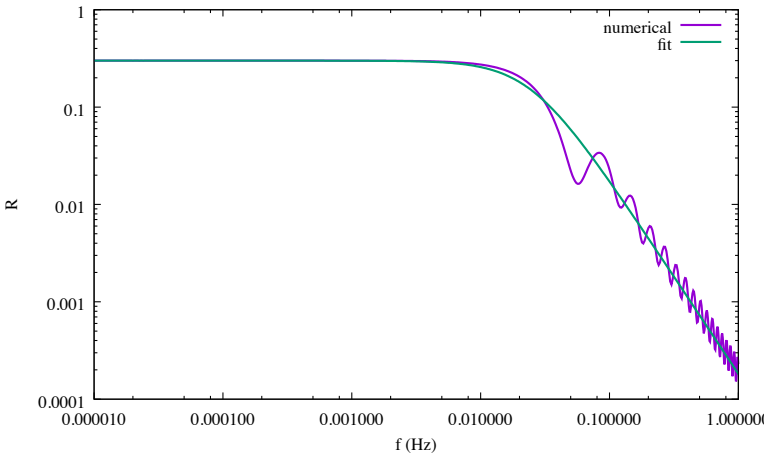

Figure 2: The signal transfer function $\mathcal{R}(f)$ for the combination of two Michelson-style LISA data channels, and the analytic fit from equation (9).

Note that the Michelson-style response has four contributions from the optical metrology noise and sixteen from the test mass acceleration noise. We convert from displacement to strain by dividing by the round-trip light travel distance $2L$, so, for example, the factor of $4P_{\rm OMS}$ gets divided by $(2L)^2$, leading to the expression seen in (12). The same factor of $1/(2L)$ is also applied to the path-length change caused by the gravitational wave, so it cancels out in the likelihood function and the SNR, and the choice to divide by $2L$ is an unimportant convention. A good analytic model for the sensitivity curve that is sufficient for most purposes is given by combining (9) and (12):

$$S_n(f) = \frac{10}{3L^2}\left(P_{\rm OMS} + 2(1+\cos^2(f/f_*))\frac{P_{\rm acc}}{(2\pi f)^4}\right)\left(1+\frac{6}{10}\left(\frac{f}{f_*}\right)^2\right) . \tag{13}$$

In addition to the instrument noise, unresolved galactic binaries will act as an effective noise source (though one that is not stationary). The galactic confusion noise goes down as the mission progresses and more foreground sources are removed. Estimates for the confusion noise using the new LISA design are given in Ref. [6], and are well fit by the function

$$S_c(f) = A\, f^{-7/3}\, e^{-f^\alpha + \beta f \sin(\kappa f)}\, [1+\tanh(\gamma(f_k - f))]\ {\rm Hz}^{-1} \tag{14}$$

with fit parameters given in Table 1. Note that the amplitude quoted here is half the value quoted in Ref. [6] since here we are using two-channel sensitivity curves. The full sensitivity curve is found by adding $S_c(f)$ to $S_n(f)$.

Figure 4 shows the contribution of the galactic confusion noise assuming a 4-year mission, along with the updated sensitivity curve that includes the confusion noise. Note that the confusion noise shown here is an average value - in practice it will vary over a year as the LISA antenna pattern sweeps across the galaxy.

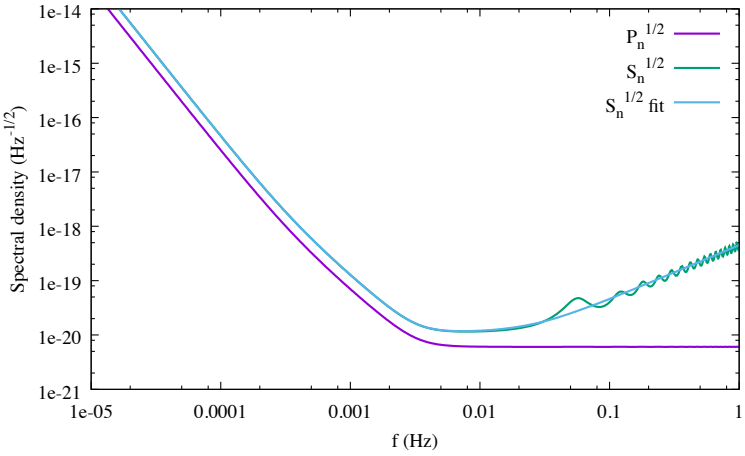

Figure 3: The amplitude spectral density of the noise, and the corresponding sensitivity curve, found by dividing $P_n(f)$ by $\mathcal{R}(f)$. The analytic fit to $Sn(f)$ given in equation (1) is also shown.

	6 mo	1 yr	2 yr	4 yr
α	0.133	0.171	0.165	0.138
β	243	292	299	-221
κ	482	1020	611	521
γ	917	1680	1340	1680
f_k	0.00258	0.00215	0.00173	0.00113

Table 1: Parameters of the analytic fit the Galactic confusion noise as described by equation (14). The amplitude A has been fixed to 9×10^{-45}. Note that the knee frequency f_k decreases with observation time and γ increase with observation time, leading to a steeper drop off in confusion noise.

2 Binary Sources

The majority of LISA sources will be binaries of various masses and mass ratios. For simplicity we will focus here on quasi-circular, non-spinning comparable mass binaries, and only consider the dominant quadrupole harmonic. Extreme mass ratio binaries, which may be highly eccentric, require a more involved treatment. While we ignore spin, the signal-to-noise ratios we compute should be good to within a factor of two or so for spinning systems. Our model for the waveforms is then

$$\begin{aligned} \tilde{h}_+(f) &= A(f)\frac{(1+\cos^2\iota)}{2}\, e^{i\Psi(f)} \\ \tilde{h}_\times(f) &= iA(f)\cos\iota\, e^{i\Psi(f)}\,, \end{aligned} \tag{15}$$

where ι describes the inclination of the orbit relative to the line of sight, and $A(f)$ and $\Psi(f)$ are the amplitude and phase of the wave. To compute the SNR we only need to know $A(f)$, and in

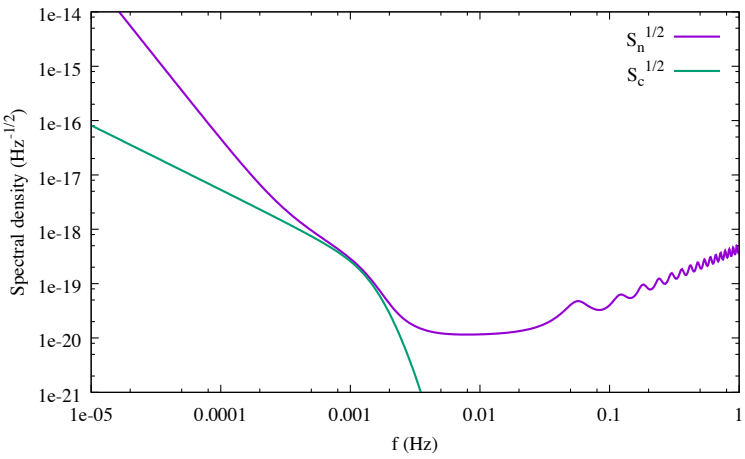

Figure 4: The amplitude spectral density of the galactic noise, $S_c^{1/2}$, and the full sensitivity curve combining the instrument noise and the galactic confusion noise, $S_n^{1/2}$, for a 4-year mission lifetime.

some cases, how the frequency evolves with time, $f(t)$.

Earlier we related the sky and polarization averaged power spectral density of the signal to the power spectral density seen in the detector via equation (4). For binary systems it is natural to extend the angle averaging to include the inclination angle:

$$\langle \tilde{h}(f)\tilde{h}^*(f)\rangle = \mathcal{R}(f)A^2(f)\frac{1}{2}\int_{-1}^{1}\left(\frac{(1+x^2)^2}{4}+x^2\right)dx = \frac{4}{5}\mathcal{R}(f)A^2(f)\,. \tag{16}$$

Note that for LIGO we recover the well-known pre-factor $\sqrt{(4/5)\mathcal{R}(f)} = 2/5$ that is applied to the GW amplitude to account for averaging over the source location and orientation [7].

The amplitude signal-to-noise ratio ρ for a deterministic signal $\tilde{h}(f)$ is given by

$$\rho^2 = 4\int \frac{|\tilde{h}(f)|^2}{P_n(f)}\,df = 4\int_{f=0}^{\infty}\frac{f|\tilde{h}(f)|^2}{P_n(f)}\,d(\ln f)\,. \tag{17}$$

Averaging over sky location, inclination and polarization we have

$$\overline{\rho^2} = \frac{16}{5}\int \frac{fA^2(f)}{S_n(f)}\,d(\ln f) = \int \frac{(2fT)S_h(f)}{S_n(f)}\,d(\ln f)\,, \tag{18}$$

Where T is the observation time and $S_h(f)$ is the one-sided, angle averaged, power spectral density of the signal,

$$S_h(f) = \frac{2\langle \tilde{h}(f)\tilde{h}^*(f)\rangle}{T}\,. \tag{19}$$

If you took a Fourier transform of the data, $d = h + n$, then ignoring any correlations between the signal and the noise, the power spectral density of the data would equal to $S_d(f) = S_h(f) + S_n(f)$.

In other words, $S_h(f)$ is the power spectral density of the signal. The factor of $(2fT)$ that appears in the expression for the optimal signal-to-noise shows that the signal is effectively boosted relative to the noise by using templates to coherently extract the signal. Rather than plotting the signal power directly (which often lies below the sensitivity curve), the convention is to plot $h_{\rm eff}^2 = (2fT)S_h(f)$, to account for the boost we get from the coherent signal extraction.

For the waveform model we use the original phenomenological inspiral-merger-ringdown (IMR) model, known as PhenomA [8]. While more accurate models now exist, such as the latest PhenomP model [9, 10], which includes spin-precession, PhenomA is good enough for making graphs and estimating SNRs. The PhenomA amplitude is given by

$$A(f) \;\equiv\; \sqrt{\frac{5}{24}}\frac{(G\mathcal{M}/c^3)^{5/6} f_0^{-7/6}}{\pi^{2/3}(D_L/c)} \begin{cases} \left(\frac{f}{f_0}\right)^{-7/6} & \text{if } \; f < f_0 \\ \left(\frac{f}{f_0}\right)^{-2/3} & \text{if } \; f_0 \le f < f_1 \\ w\,\mathcal{L}\,(f,\, f_1,\, f_2) & \text{if } \; f_1 \le f < f_3\,, \end{cases} \tag{20}$$

where

$$f_k \equiv \frac{a_k\eta^2 + b_k\eta + c_k}{\pi(GM/c^3)}\,, \tag{21}$$

$$\mathcal{L}(f, f_1, f_2) \equiv \left(\frac{1}{2\pi}\right)\frac{f_2}{(f-f_1)^2 + f_2^2/4}\,, \tag{22}$$

and

$$w \equiv \frac{\pi f_2}{2}\left(\frac{f_0}{f_1}\right)^{2/3}\,. \tag{23}$$

Here $M = m_1 + m_2$ is the total mass, $\eta = m_1 m_2/M^2$ is the symmetric mass ratio and $\mathcal{M} = (m_1 m_2)^{3/5}/M^{1/5}$ is the chirp mass. The G's and c's have been included for those that are not used to working in natural units. Note that the combinations GM/c^3 and D_L/c both have units of time. A useful number to remember is that the mass of the Sun, $GM_\odot/c^3$, is approximately 5 microseconds in natural units. The coefficients for the transition frequencies f_k are given in Table 2. Roughly speaking, f_0 is the merger frequency, f_1 is the ringdown frequency, f_2 is decay-width of the ringdown and f_3 is the cut-off frequency.

	a_k	b_k	c_k
f_0	2.9740×10^{-1}	4.4810×10^{-2}	9.5560×10^{-2}
f_1	5.9411×10^{-1}	8.9794×10^{-2}	1.9111×10^{-1}
f_2	5.0801×10^{-1}	7.7515×10^{-2}	2.2369×10^{-2}
f_3	8.4845×10^{-1}	1.2848×10^{-1}	2.7299×10^{-1}

Table 2: Polynomial coefficients of the transition frequencies.

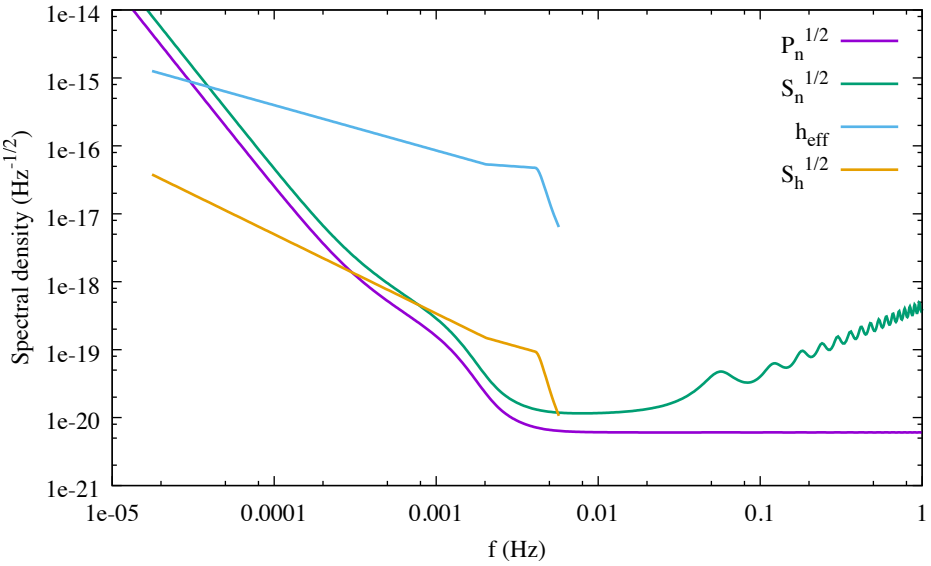

Figure 5: The amplitude spectral density of the noise $\sqrt{P_n}$, and the amplitude sensitivity curve $\sqrt{S_n}$ are plotted against the raw strain spectral density $\sqrt{S_h}$ and the effective strain spectral density $h_{\rm eff}$ for an equal mass black hole binary at $z = 3$ with source frame total mass $M = 10^6\,M_\odot$. This system is so bright that even its raw amplitude will be visible in the detector. However, the effective amplitude $h_{\rm eff}$ that appears in the numerator of the SNR calculation better communicates the true brightness of the source. The area between the $h_{\rm eff}$ curve and the $S_n^{1/2}$ curve roughly corresponding to the optimal SNR of 2626. Note that this graph differs slightly from the one shown in Figure 1, which plots dimensionless characteristic strain $h_c(f) = \sqrt{fS(f)}$ rather than strain spectral density $\sqrt{S}$.

The final ingredient we need to compute the SNR is the frequency range covered by the signal. For comparable mass black holes, with $M > 10^4 M_\odot$, the signal will sweep across the LISA band and merge in less than the mission lifetime. However, for lower mass systems, such as stellar mass black holes that will merger in the LIGO band a decade or so later, or for white dwarf binaries, which may be millions of years from merger, we need to specify the start and end frequencies for the SNR integration. To leading post-Newtonian order, the frequency as a function of time is given by

$$f(t) = \frac{1}{8\pi(G\mathcal{M}/c^3)}\left(\frac{5(G\mathcal{M}/c^3)}{t-t_c}\right)^{3/8}\,, \tag{24}$$

where t_c is the time of coalescence. For example, an equal mass binary at $z = 3$ with a total source-frame mass of $M = 10^6\,M_\odot$ will have a GW frequency of 2.93×10^{-5} Hz one year prior to merger. Note that it is the detector frame mass, $M_z = M(1+z)$, that should be used in equations (20) and (24). For these high mass systems it makes sense to plot $h_{\rm eff}$ across the entire LISA band, and not worry about setting limits in the SNR integration. Tracks in $\sqrt{S_h}$ and $h_{\rm eff}$ for the aforementioned source are shown in Figure 5. In contrast, a source similar to GW150914 that is 5 years from merger when LISA turns on will sweep from $f = 16$ mHz to $f = 29$ mHz over the

nominal 4 year mission lifetime.

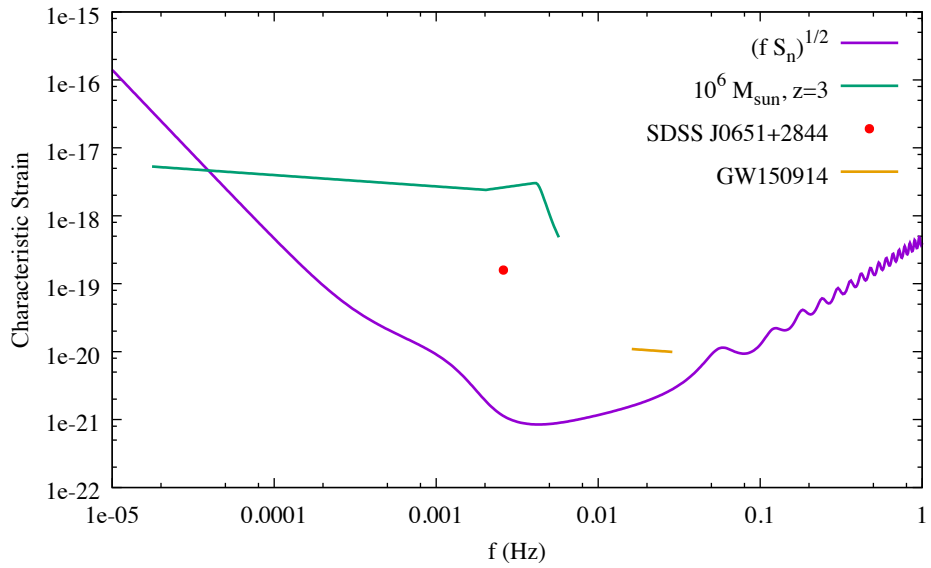

Figure 6: The sensitivity curve in terms of characteristic strain, $\sqrt{fS_n}$ is compared to three types of signal: an equal mass black hole binary at $z = 3$ with source-frame total mass $M = 10^6\,M_\odot$; the galactic verification binary SDSS J0651+2844 observed for 4 years; and a signal similar to the first LIGO detection GW150914 if the LISA observation started 5 years prior to merger and continued for 4 years.

For galactic binaries the time to merger is typically very large compared to the mission lifetime, and the frequencies will evolve very little over the course of the mission. Taylor expanding (24) we find

$$f(t) = f_{\rm in} + \frac{96}{5}\pi^{8/3}(G\mathcal{M}/c^3)^{5/3} f_{\rm in}^{11/3}(t - t_{\rm in}) + \dots\,, \tag{25}$$

where $f_{\rm in}$ is the GW frequency at the start of the observation, at time $t_{\rm in}$. For typical galactic binaries the change in frequency Δf during the mission lifetime is so small that it no longer makes sense to the plot the signals as tracks. Rather, the signals are plotted as points with an amplitude $h_{\rm GB}$ that follows from evaluating the SNR integral:

$$\overline{\rho^2} = \frac{16}{5}\int_{f_{\rm in}}^{f_{\rm in}+\Delta f} \frac{A^2(f)}{S_n(f)}\,df \approx \frac{16}{5}\frac{\Delta f A^2(f_{\rm in})}{S_n(f_{\rm in})} \equiv \frac{h_{\rm GB}^2(f_{\rm in})}{S_n(f_{\rm in})} \tag{26}$$

where

$$h_{\rm GB} = \frac{8\,T^{1/2}(G\mathcal{M}/c^3)^{5/3}\pi^{2/3} f_{\rm in}^{2/3}}{5^{1/2}(D_L/c)}\,. \tag{27}$$

For example, SDSS J0651+2844 which has $D_L \sim 1$ Kpc, $m_1 \sim 0.5\,M_\odot$, $m_2 \sim 0.25\,M_\odot$, and $f_{\rm in} = 2.6$ mHz, will produce a strain spectral density of $h_{\rm GB} = 2.8 \times 10^{18}\,{\rm Hz}^{-1/2}$ and have an SNR of 120 assuming a 4 year mission lifetime. Of course, it not strictly correct to compute

angle averaged SNRs for a source with a known sky location and orientation, nor does it make much sense to plot its amplitude against against an all-sky averaged sensitivity curve, but doing so allows us to put all LISA sources on a single graph.

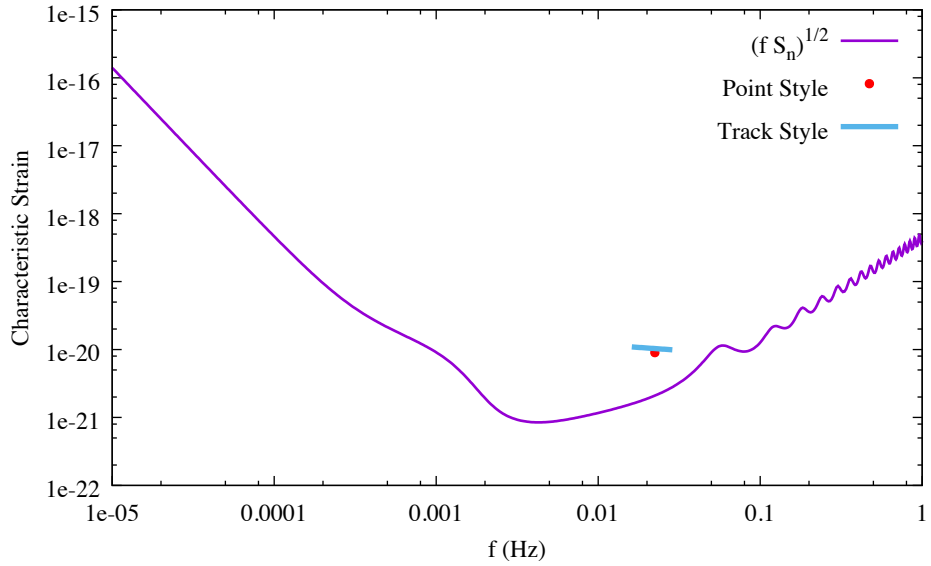

Figure 7: The characteristic strain produced by a GW150914 type system that is 20 years from merger at the beginning of the LISA observation. The track-style representation, where the SNR is estimate from the area under the curve, is compared to the point style representation used for slowly evolving white-dwarf binaries, where the SNR is given by the ratio of the height of the sensitivity curve and the hight of the point.

The differing conventions between how slowly evolving and rapidly evolving signals are plotted can be problematic for "LIGO binaries". For example, if a GW150914 type system was 20 years from merger when LISA started observations, it would be emitting at a gravitational wave frequency of 9.5 mHz, and four years later it would be emitting at 10.4 mHz, producing a track that runs for just $\Delta \ln f = 0.09$. Since the frequency range is so short, the questions becomes do we treat the system as evolving, and plot a track as we do for massive black holes, or do we treat the system as non-evolving, and plot a point as we do for galactic binaries? Figure 7 shows that the two choices paint an inconsistent picture. To arrive at consistent representations, where sources appear at almost the same height when shown as evolving tracks or non-evolving points, we recommend switching from tracks to points when $\Delta \ln f < 0.5$.

References

[1] Heather Audley et al. Laser Interferometer Space Antenna. *arXiv 1702.00786*, 2017.

[2] C. J. Moore, R. H. Cole, and C. P. L. Berry. Gravitational-wave sensitivity curves. *Class. Quant. Grav.*, 32(1):015014, 2015. doi: 10.1088/0264-9381/32/1/015014.

[3] Shane L. Larson, William A. Hiscock, and Ronald W. Hellings. Sensitivity curves for space-borne gravitational wave interferometers. *Phys. Rev.*, D62:062001, 2000. doi: 10.1103/PhysRevD.62.062001.

[4] Neil J. Cornish. Detecting a stochastic gravitational wave background with the Laser Interferometer Space Antenna. *Phys. Rev.*, D65:022004, 2002. doi: 10.1103/PhysRevD.65.022004.

[5] Thomas A. Prince, Massimo Tinto, Shane L. Larson, and J. W. Armstrong. The LISA optimal sensitivity. *Phys. Rev.*, D66:122002, 2002. doi: 10.1103/PhysRevD.66.122002.

[6] Neil Cornish and Travis Robson. Galactic binary science with the new LISA design. *J. Phys. Conf. Ser.*, 840(1):012024, 2017. doi: 10.1088/1742-6596/840/1/012024.

[7] Lee Samuel Finn and David F. Chernoff. Observing binary inspiral in gravitational radiation: One interferometer. *Phys. Rev.*, D47:2198–2219, 1993. doi: 10.1103/PhysRevD.47.2198.

[8] Parameswaran Ajith et al. Phenomenological template family for black-hole coalescence waveforms. *Class. Quant. Grav.*, 24:S689–S700, 2007. doi: 10.1088/0264-9381/24/19/S31.

[9] Mark Hannam. Modelling gravitational waves from precessing black-hole binaries: Progress, challenges and prospects. *Gen. Rel. Grav.*, 46:1767, 2014. doi: 10.1007/s10714-014-1767-2.

[10] Patricia Schmidt, Frank Ohme, and Mark Hannam. Towards models of gravitational waveforms from generic binaries II: Modelling precession effects with a single effective precession parameter. *Phys. Rev.*, D91(2):024043, 2015. doi: 10.1103/PhysRevD.91.024043.